

Permutation-Invariant Graph Partitioning: How Graph Neural Networks Capture Structural Interactions?

Asela Hevapathige¹ Qing Wang¹

¹ Graph Research Lab, School of Computing, Australian National University

Abstract

Graph Neural Networks (GNNs) have paved the way for being a cornerstone in graph-related learning tasks. Yet, the ability of GNNs to capture structural interactions within graphs remains under-explored. In this work, we address this gap by drawing on the insight that permutation invariant graph partitioning enables a powerful way of exploring structural interactions. We establish theoretical connections between permutation invariant graph partitioning and graph isomorphism, and then propose Graph Partitioning Neural Networks (GPNNs), a novel architecture that efficiently enhances the expressive power of GNNs in learning structural interactions. We analyze how partitioning schemes and structural interactions contribute to GNN expressivity and their trade-offs with complexity. Empirically, we demonstrate that GPNNs outperform existing GNN models in capturing structural interactions across diverse graph benchmark tasks.

1. Introduction

Graph Neural Networks (GNNs) have emerged as the *de facto* standard for tackling graph learning tasks (Horn et al., 2022; Bodnar et al., 2021; Bouritsas et al., 2022). Among the rich landscape of GNN models, Message-Passing Neural Networks (MPNNs) stand out for their simplicity and efficiency, making them a popular choice for real-world applications. This is due to their ability to leverage local neighborhood information through a message-passing scheme, which iteratively computes node representations (Gilmer et al., 2017; Kipf & Welling, 2017).

However, the representational power of MPNNs is fundamentally constrained by the Weisfeiler-Lehman test (1-WL) (Weisfeiler & Leman, 1968b; Xu et al., 2018; Morris et al., 2019). To overcome this limitation, researchers have proposed various approaches to enhance MPNN expressivity beyond 1-WL, including injecting structural properties (Bouritsas et al., 2022; Barceló et al., 2021; Wijesinghe & Wang,

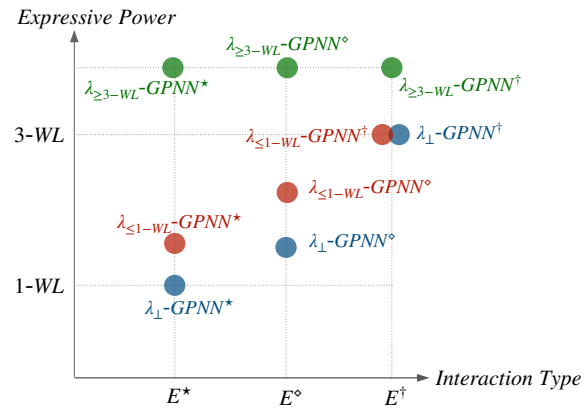


Figure 1: The expressivity of GPNN variants is analysed in terms of (1) *interaction type*: E^* (intra-edges), E° (intra-edges and inter-edges), and E^\dagger (all edges); (2) *expressive power*: 1-WL and 3-WL, under different permutation-invariant graph partitioning schemes λ_\perp , $\lambda_{\leq 1-WL}$, and $\lambda_{\geq 3-WL}$. Detailed theoretical results are provided in the section ‘‘Expressivity Analysis’’.

2022; Xu et al., 2024), incorporating higher-order substructures (Morris et al., 2019; 2020b; Abu-El-Haija et al., 2019), expanding receptive fields for message passing (Nikolentzos et al., 2020; Feng et al., 2022; Wang et al., 2022), leveraging subgraphs (Zhao et al., 2022a; Zhang & Li, 2021; Wang & Zhang, 2022; Bevilacqua et al., 2022; Cotta et al., 2021), integrating homomorphism counts (Zhang et al., 2024b; Jin et al., 2024) and applying inductive coloring techniques (You et al., 2021; Huang et al., 2023). Despite these advancements, there is still limited understanding of how structural components within a graph, such as subgraphs representing diverse properties, interact and influence expressivity in learning tasks. Existing methods primarily focus on straightforward interactions between nodes and their neighbors, leaving the intricate interplay among structural components underexplored. Addressing these gaps is crucial for unlocking the full potential of expressive GNNs.

Present work. We aim to address the aforementioned limitations by observing that partitioning a graph into sub-

graphs that preserve structural properties provides a powerful means to exploit interactions among different structural components of the graph. Notably, graphs in real-world applications often consist of various structural components that can be distinguished by their topological properties. By exploring these structural components and their interactions, we can gain novel insights into the structure of a graph and enhance the power of graph representations.

Nevertheless, unlike other data types such as images or sequences, graphs lack an inherent, consistent ordering of vertices. Therefore, a model that learns representations of graphs must treat isomorphic graphs – those that differ only by vertex permutations – as identical. To achieve this, ensuring permutation invariance is crucial during graph partitioning. This guarantees that graphs are divided based on their intrinsic structural properties, rather than being influenced by arbitrary vertex orderings.

Inspired by these insights, we explore how permutation-invariant graph partitioning enhances GNN expressivity efficiently. Our key contributions are:

- **Theoretical insights:** We establish a novel connection between graph partitioning and graph isomorphism by introducing the concepts of *partition isomorphism* and *interaction isomorphism*, providing a rigorous theoretical framework for analyzing structural interactions.
- **GNN architecture:** We propose *Graph Partitioning Neural Networks* (GPNNs), a new GNN architecture that integrates structural interactions through permutation-invariant graph partitioning to enhance graph representation learning.
- **Expressivity analysis:** We theoretically prove that GPNNs surpass the expressive power of 1-WL and efficiently approach the expressive power of 3-WL, addressing critical limitations of traditional GNNs.
- **Complexity analysis:** We show that GPNN variants achieve a balance between computational efficiency and representational power, making them practical for large-scale graph learning tasks.
- **Practical partitioning:** We explore efficient, permutation-invariant graph partitioning schemes, such as k -core and degree-based partitioning, to enable meaningful subgraph extraction and preserve structural properties.

Figure 1 illustrates the theoretical results on the expressivity of the proposed GPNN architecture in relation to k -WL (Cai et al., 1992) and interaction types across different graph partitioning schemes. To empirically verify the theoretical designs of GPNN, we conduct experiments on diverse graph benchmark tasks, demonstrating its superior performance over state-of-the-art models.

2. Related Work

GNNs beyond 1-WL. The Weisfeiler-Lehman algorithm (Weisfeiler & Leman, 1968a) has commonly been used as a yardstick for measuring the expressive power of GNNs. Since Xu et al. (2018); Morris et al. (2019) showed that the expressive power of standard GNNs is upper-bounded by 1-WL, numerous studies have explored the connections between the k -WL hierarchy (Cai et al., 1992) and the expressive power of GNNs (Zhao et al., 2022b), which has led to the development of higher-order GNNs (Maron et al., 2019b; Morris et al., 2019; 2020b; Zhao et al., 2022b). Apart from higher-order GNNs, there are a variety of GNN models proposed in the literature, which enhance the expressive power of MPNNs to go beyond 1-WL. Some of these models extract structural information using a pre-processing step and inject structural information into a message-passing scheme as node or edge features (Horn et al., 2022; Barceló et al., 2021; Bouritsas et al., 2022; Wijesinghe & Wang, 2022). Some models apply base GNNs such as GIN (Xu et al., 2018) at a subgraph level rather than the entire graph based on the observation that 1-WL indistinguishable graphs may contain 1-WL distinguishable subgraphs (Bevilacqua et al., 2022; Cotta et al., 2021; Zeng et al., 2023; Frasca et al., 2022). We refer the reader to the survey articles by Sato (2020) and Zhang et al. (2024a) for a detailed discussion on expressive GNNs.

Partitioning-based GNNs. Graph partitioning has previously been explored in the domain of GNNs. Several works have employed partitioning for speeding up large-scale graph processing (Mu et al., 2023; Gaunt et al., 2018; Miao et al., 2021; Chiang et al., 2019; Lin, 2021; Yang et al., 2023; Wan et al., 2023), graph similarity computation (Xu et al., 2021; 2020), and graph matching (Ye et al.; He et al., 2021). The main idea of these works is to use partitioning techniques to divide graphs into smaller components, which reduces memory and computational requirements during model training. This approach also enables parallel processing and reduces model parameter space, leading to faster training and potentially better representations for large-scale graphs.

Our work fundamentally differs from existing partitioning based GNNs by focusing on representation learning rather than computational efficiency. We employ permutation-invariant graph partitions to uncover structural interactions within and between components, encoding these intersections into graph representations. To our knowledge, no prior studies have explored how graph partitioning can be integrated into representation learning to capture structural interactions within graphs. Given that permutation invariance is a fundamental inductive bias in graph learning, a key challenge lies in incorporating graph partitioning into representation learning while preserving the permutation-

How Graph Neural Networks Capture Structural Interactions?

	Type	Pairs of Graphs	
		(a)	(b)
Example graph pairs		G_1	H_1
Boundary subgraphs	Graph Isomorphism		
Partitioned subgraphs	Interaction Isomorphism		
	Partition Isomorphism		

Figure 2: Two pairs of non-isomorphic graphs, (G_1, H_1) and (G_2, H_2) , are partitioned by node degrees, grouping nodes with the same degree. Boundary and partitioned subgraphs are shown, with different subgraphs highlighted in red and blue. (a) $G_1 \xrightarrow{PI} H_1$ and $G_1 \xrightarrow{II} H_1$; (b) $G_2 \xrightarrow{PI} H_2$, but $G_2 \xrightarrow{II} H_2$.

invariance properties of graphs. This work is the first to tackle this challenge and to explore the connection between permutation-invariant graph partitioning and graph isomorphism to enhance the expressive power of GNNs.

3. Graph Partitioning Scheme

In this section, we define permutation-invariant graph partitioning and explain its connection to graph isomorphism.

Let G be a simple graph, and $V(G)$ and $E(G)$ refer to the vertex set and the edge set of G , respectively. Given $d \in \mathbb{N}$, for each $v \in V(G)$, the set of d -hop neighbouring vertices is denoted as $N_d(v) = \{u \in V(G) \mid (u, v) \in E(G), \delta(u, v) \leq d\}$, where $\delta(u, v)$ refers to the shortest-path distance between two vertices u and v . When d is equal to 1, we denote it as $N(v)$. An induced subgraph of G by $U \subseteq V(G)$ is the graph $G[U]$ with a vertex set U and edges only between vertices in U , denote as $G[U] \subseteq G$.

Two graphs G_1 and G_2 are *isomorphic*, denoted as $G_1 \simeq G_2$, if there exists a bijection $g : V(G_1) \rightarrow V(G_2)$ such that $(v, u) \in E(G_1)$ if and only if $(g(v), g(u)) \in E(G_2)$. A permutation π on a graph G is a bijection $\pi : V(G) \rightarrow V(G)$ such that $\pi(G) = (V(G), \pi(E(G)))$, where $\pi(E(G)) = \{(\pi(v), \pi(u)) \mid (v, u) \in E(G)\}$. A function f is *permutation-invariant* if and only if $f(G) = f(\pi(G))$ for any graph G and any permutation π on G . Let \mathcal{G} be a set of graphs closed under isomorphism. A *subgraph invariant* is a function $\phi : \mathcal{G} \rightarrow \mathcal{G}$ that determines a subgraph $\phi(G) \subseteq G$ for each $G \in \mathcal{G}$, preserved under isomorphisms.

Definition 3.1 (Graph Partitioning Scheme). Let $P(\mathcal{G})$ be the powerset of \mathcal{G} and $\Phi = \{\phi_j\}_{j \in [1, k]}$ be a family of subgraph invariants. A *graph partitioning scheme* is a permutation invariant function $f_\Phi : \mathcal{G} \rightarrow P(\mathcal{G})$ which partitions any graph $G \in \mathcal{G}$ into a set of subgraphs $\{S_1, \dots, S_k\}$, where $\bigcup_{1 \leq i \leq k} V(S_i) = V(G)$, $\bigwedge_{1 \leq i \neq j \leq k} V(S_i) \cap V(S_j) = \emptyset$,

and $\phi_j(G) = S_j$ for $j \in [1, k]$. Note that S_j can be an empty subgraph, i.e., $V(S_j) = \emptyset$ and $E(S_j) = \emptyset$.

The permutation-invariant property of a graph partitioning scheme is crucial for exploring structural interactions. This property not only ensures that interactions among different structural components are consistently captured, under any vertex reordering, but also enables meaningful comparisons between subgraphs with the same indices, partitioned from different graphs by the same graph partition scheme through a family of subgraph invariants.

Based on graph partitioning schemes, we define two notions of isomorphism on graphs: one characterizes interactions within partitioned subgraphs and the other characterizes interactions across partitioned subgraphs.

Definition 3.2 (Partition-Isomorphism). Two graphs G and G' are *partition-isomorphic*, denoted as $G \xrightarrow{PI} G'$, with respect to a partitioning scheme f_Φ if there exists a bijective function $g : f_\Phi(G) \rightarrow f_\Phi(G')$ such that $f_\Phi(G) = \{S_1, \dots, S_k\}$, $f_\Phi(G') = \{S'_1, \dots, S'_k\}$, and $g(S_i) \simeq S'_i$ for $i = 1, \dots, k$.

A vertex $v \in V(G)$ is a *border vertex* with respect to f_Φ if there exist two subgraphs $\{S_i, S_j\} \subseteq f_\Phi(G)$ such that $(v, u) \in E(G)$, $v \in V(S_i)$, $u \in V(S_j)$ and $S_i \neq S_j$. We use $V_B(G)$ to denote the set of all border vertices in G .

Definition 3.3 (Boundary Subgraph). The *boundary subgraph* $B(G) = (V, E)$ of a graph G with respect to f_Φ is defined by the vertex set $V = V_B(G)$ and the edge set $E = \{(v, u) \in E(G) \mid v, u \in V_B(G)\}$, where each edge in E connects two border vertices.

Boundary subgraphs underpin structural interaction equivalence in partitioned graphs.

Definition 3.4 (Interaction-Isomorphism). Two graphs G and G' are *interaction-isomorphic*, denoted $G \xrightarrow{II} G'$, with

respect to a partitioning scheme f_Φ , if and only if:

- $G \xrightarrow{PI} G'$, i.e., graphs are partition-isomorphic under f_Φ ;
- $B(G) \simeq B(G')$, i.e., boundary subgraphs are isomorphic.

The following establishes the connection between partition-isomorphism, interaction-isomorphism, and graph isomorphism. One direction of the proof follows directly from the definitions, while the other is shown using counterexample graphs in Figure 2. A detailed proof is in the Appendix.

Theorem 3.5. *Fix a graph partitioning scheme. We have:*

(a) *If $G \simeq G'$, then $G \xrightarrow{II} G'$, but not vice versa;* (b) *If $G \xrightarrow{II} G'$, then $G \xrightarrow{PI} G'$, but not vice versa.*

4. Proposed GNN Architecture

In this section, we introduce *Graph Partitioning Neural Networks* (GPNN), a novel GNN model which can integrate structural interactions into representation learning.

We begin by defining partitioning colouring, where vertices and edges are assigned colours to reflect permutation-invariant partitions generated by a graph partition scheme.

Definition 4.1 (Partition Colouring). Let C_V be a set of vertex colours, C_E be a set of edge colours containing $\{c_e, c_a, c_n\}$, $C_V \cap C_E = \emptyset$, $\{S_1, \dots, S_k\}$ be a set of subgraphs generated by a graph partitioning scheme over G , and $\pi(\cdot)$ be an injective hashing function. A *partition colouring* $\lambda = (\lambda_V, \lambda_E)$ consists of the following:

- *Vertex colouring*: Each vertex $v \in V(G)$ is assigned a *vertex colour*, $\lambda_V : V(G) \rightarrow C_V$ such that $\lambda_V(v) = \lambda_V(u)$ if and only if $v \in V(S_i)$ and $u \in V(S_i)$.
- *Edge colouring*: Each pair of distinct vertices $\{v, u\} \subseteq V(G)$ is assigned an *edge colour*, $\lambda_E : V(G) \times V(G) \rightarrow C_E$ such that

$$\lambda_E(v, u) = \begin{cases} \pi(\lambda_V(v), c_e, \lambda_V(u)) & (v, u) \in E(G), \lambda_V(v) = \lambda_V(u); \\ \pi(\lambda_V(v), c_a, \lambda_V(u)) & (v, u) \in E(G), \lambda_V(v) \neq \lambda_V(u); \\ \pi(\lambda_V(v), c_n, \lambda_V(u)) & (v, u) \notin E(G). \end{cases}$$

Here, $\{c_e, c_a, c_n\}$ represents three types of interactions: *inter-interaction*, *intra-interaction*, and *non-interaction*, respectively. Intuitively, inter-interactions refer to interactions between vertices within the same partitioned subgraph, intra-interactions refer to interactions between vertices across different partitioned subgraphs, and non-interactions indicate that no direct interactions occurs between vertices.

Definition 4.2 (Coloured Neighbourhood). For each vertex $v \in V(G)$, the neighbourhood $N_d(v)$ consists of a set of neighbouring vertex subsets $\{N_d^1(v), \dots, N_d^k(v)\}$, each of

which is coloured with a distinct colour under λ_V such that, for any two vertices $\{u, w\} \subseteq N_d(v)$, $\lambda_V(u) = \lambda_V(w)$ if and only if $\{u, w\} \subseteq N_d^j(v)$ for exactly one $j \in [1, k]$.

Below we present the message-passing scheme of GPNN. Given a partition colouring $\lambda = (\lambda_V, \lambda_E)$, let $\beta_v^{(0)} = \lambda_V(v)$ and $\gamma_v^{(0)} = \lambda_V(v)$ for any $v \in V(G)$ and $\alpha_{vu}^{(0)} = \lambda_E(v, u)$ for any $v, u \in V(G)$. We learn the vertex embedding $\beta_v^{(\ell+1)}$ of each vertex v at the $(\ell + 1)$ -th iteration as

$$\beta_v^{(\ell+1)} = \text{UPD}\left(\gamma_v^{(\ell)}, \text{AGG}\{\gamma_u^{(\ell)} | u \in N(v)\}\right). \quad (1)$$

$\text{UPD}(\cdot)$ and $\text{AGG}(\cdot)$ are injective and permutation-invariant functions that represent update and aggregate operations in GNNs, respectively. Then, we define the interaction embedding $\alpha_{vu}^{(\ell+1)}$ of (v, u) at the $(\ell + 1)$ -th iteration as

$$\alpha_{vu}^{(\ell+1)} = \text{UPD}\left(\alpha_{vu}^{(\ell)}, \text{AGG}\left(\{\alpha_{vw}^{(\ell)}, \alpha_{uw}^{(\ell)} | w \in N_d(v)\}\right)\right). \quad (2)$$

We then aggregate the embeddings of neighboring vertices and their corresponding interaction embeddings from different partitions (i.e., the coloured neighbourhood $\{N_d^1(v), \dots, N_d^k(v)\}$) into a combined embedding γ_v as

$$\gamma_v^{(\ell+1)} = \text{CMB}\left(\text{AGG}\left(\{(\beta_u^{(\ell+1)}, \alpha_{vu}^{(\ell+1)}) | u \in N_d^1(v)\}\right), \dots, \text{AGG}\left(\{(\beta_u^{(\ell+1)}, \alpha_{vu}^{(\ell+1)}) | u \in N_d^k(v)\}\right)\right). \quad (3)$$

$\text{CMB}(\cdot)$ is an injective combining function, closed under permutation. Note that (v, u) of $\alpha_{vu}^{(\ell+1)}$ may correspond to inter-interaction, intra-interaction, or non-interaction, depending on not only how v and u are connected in G but also how they are partitioned by a graph partitioning scheme.

Remark 4.3. Our model can be integrated into any existing GNN models as a plugin. Let h_v^{gnn} be a node embedding from an existing GNN model (e.g., GIN (Xu et al., 2018) and GCN (Kipf & Welling, 2017)). By combining h_v^{gnn} with $\gamma_v^{(\ell+1)}$, we obtain the representation for each vertex v as

$$h_v = \text{CMB}\left(h_v^{gnn}, \gamma_v^{(\ell+1)}\right). \quad (4)$$

An illustration of the high-level workflow of GPNN is provided in Figure 3.

5. Expressivity Analysis

We discuss the expressivity of GPNN from two aspects: (1) How does a partition colouring, determined by a chosen graph partitioning scheme, affect the expressivity of GPNN? (2) How do different types of interactions affect the expressivity of GPNN? Detailed proofs for theorems and lemmas presented in this section are included in the Appendix.

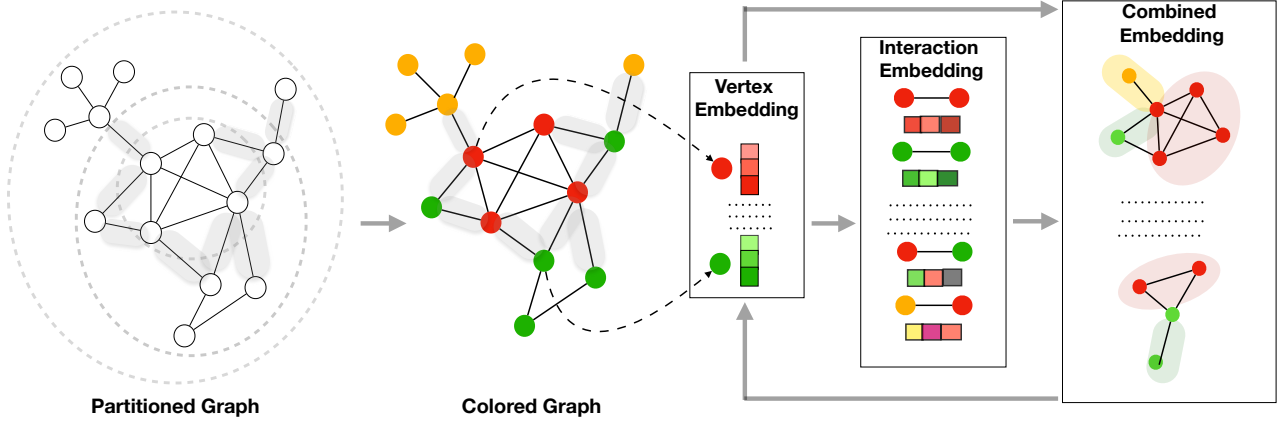


Figure 3: A high-level workflow of $\lambda_{\text{core}}\text{-GPNN}$ for an input graph. The intra-edges are marked using grey color. GPNN generates vertex representations by considering interactions within and between partitions.

We use $\lambda\text{-GPNN}^\delta$ to refer to the variants of GPNN with a partition colouring λ , $d = 1$ (i.e., $N_d(v)$ contains direct neighbours of v and v itself), and $\delta \in \{\star, \diamond, \dagger\}$, where \star , \diamond , and \dagger denote that (v, u) in Equation (2) considers intra-interactions (E^\star), both inter-interactions and intra-interactions (E^\diamond), and all interactions (E^\dagger), respectively. We also introduce the notion of λ -equivalence to compare the expressivity of different graph partitioning schemes.

Definition 5.1 (λ -Equivalence). Let $\lambda = (\lambda_V, \lambda_E)$ be a partition colouring. Two graphs G and H are λ -equivalent, denoted as $G \equiv_\lambda H$, if they are indistinguishable by λ , i.e.,

- for each $c \in C_V$, $|\{v \in V(G) | \lambda_V(v) = c\}| = |\{v' \in V(H) | \lambda_V(v') = c\}|$;
- for each $c \in C_E$, $|\{\{v, u\} \subseteq V(G) | \lambda_E(v, u) = c\}| = |\{\{v', u'\} \subseteq V(H) | \lambda_E(v', u') = c\}|$.

Given two partition colourings λ_1 and λ_2 , we say that λ_1 is at least as expressive as λ_2 , denoted as $\lambda_1 \supseteq \lambda_2$, if and only if for any two graphs $\{G, H\} \subseteq \mathcal{G}$, $G \equiv_{\lambda_2} H$ whenever $G \equiv_{\lambda_1} H$. Similarly, we use $\lambda_1 \sqsupset \lambda_2$ and $\lambda_1 \equiv \lambda_2$ to indicate that λ_1 is strictly more expressive than or equally expressive as λ_2 , respectively. These notations can also be extended to k -WL and GPNNs.

A partition colouring is *trivial*, denoted as λ_\perp , if $f_\Phi(G) = \{G\}$ for any $G \in \mathcal{G}$, i.e., all vertices assigned the same colour. A partition colouring is *complete*, denoted as λ_\top , if $f_\Phi(G) = f_\Phi(H) \Leftrightarrow G \simeq H$ for any $\{G, H\} \subseteq \mathcal{G}$, i.e., orbit colouring (McKay & Piperno, 2014). The expressivity of a partition colouring λ is lower bounded by λ_\perp and upper bounded by λ_\top .

The following proposition describes how the expressivity of $\lambda\text{-GPNN}^\delta$ compares to 1-WL and 3-WL when λ is trivial. The expressive power of $\lambda_\perp\text{-GPNN}^\delta$ is at least as expressive as 1-WL but upper bounded by 3-WL.

Proposition 5.1. *The following hold:* (1) $\lambda_\perp\text{-GPNN}^\star \equiv 1\text{-WL}$; (2) $\lambda_\perp\text{-GPNN}^\star \sqsubseteq \lambda_\perp\text{-GPNN}^\diamond \sqsubseteq \lambda_\perp\text{-GPNN}^\dagger$; (3) $\lambda_\perp\text{-GPNN}^\dagger \sqsubseteq 3\text{-WL}$.

When considering the same interaction type, GPNN $^\delta$ maintains the expressivity order of their respective partition colourings, as stated in the theorem below.

Theorem 5.2. *Let λ_1 and λ_2 be two partition colourings with $\lambda_1 \sqsupseteq \lambda_2$. Then $\lambda_1\text{-GPNN}^\delta \sqsupseteq \lambda_2\text{-GPNN}^\delta$ for any $\delta \in \{\star, \diamond, \dagger\}$.*

The following proposition establishes expressivity bounds of $\lambda\text{-GPNN}^\delta$ in terms of the partition colouring λ and k -WL. For clarity, we define $\max(\lambda, k\text{-WL}) = k\text{-WL}$ if $\lambda \sqsubseteq k\text{-WL}$, or $\max(\lambda, k\text{-WL}) = \lambda$ if $\lambda \sqsupseteq k\text{-WL}$.

Theorem 5.3. *Let λ be a partition colouring satisfying $\lambda \sqsubseteq k\text{-WL}$ or $\lambda \sqsupseteq k\text{-WL}$ for some $k \in \mathbb{N}$. Then $\max(\lambda, 1\text{-WL}) \sqsubseteq \lambda\text{-GPNN}^\delta$ and $\lambda\text{-GPNN}^\delta \sqsubseteq \max(\lambda, 3\text{-WL})$ for any $\delta \in \{\star, \diamond, \dagger\}$.*

We show that for a partition coloring λ below 3-WL, the expressive power of $\lambda\text{-GPNN}^\delta$ is non decreasing when more interactions are captured into representations. However, when a partition coloring λ is at least as expressive as 3-WL, the expressive power of $\lambda\text{-GPNN}^\delta$ remains unchanged.

Lemma 5.1. *When $\lambda \sqsubset 3\text{-WL}$, $\lambda\text{-GPNN}^\dagger \sqsupseteq \lambda\text{-GPNN}^\diamond \sqsupseteq \lambda\text{-GPNN}^\star$. When $\lambda \sqsupseteq 3\text{-WL}$, $\lambda\text{-GPNN}^\dagger \equiv \lambda\text{-GPNN}^\diamond \equiv \lambda\text{-GPNN}^\star$.*

Based on Lemma 5.1, the following theorem compares the expressivity of different GPNN variants.

Theorem 5.4. *For any partition colouring λ , $\lambda\text{-GPNN}^\dagger \sqsupseteq \lambda\text{-GPNN}^\diamond \sqsupseteq \lambda\text{-GPNN}^\star$.*

Remark 5.5. The expressivity of $\lambda\text{-GPNN}^\delta$ stems from two key sources: the capacity of a chosen graph partitioning

scheme, as reflected by the partition colouring λ , and the ability to capture different types of structure interactions via $\delta \in \{\star, \diamond, \dagger\}$. The former sets the lower bound of λ -GPNN $^\delta$ in its ability to distinguish non-isomorphic graphs, ranging from a trivial colouring to a complete colouring. For the latter, λ -GPNN $^\delta$ addresses partition isomorphism and interaction isomorphism by considering various types of interactions. Inter-interactions enable λ -GPNN $^\delta$ to handle interactions within partitions, as required by partition isomorphism, while intra-interactions capture interactions across partitions, as considered by interaction isomorphism. The model capacity of GPNN $^\delta$ alone is bounded between 1-WL as a lower bound and 3-WL as an upper bound.

6. Complexity Analysis

Generally, 1-WL and traditional GNNs that are upper-bounded by 1-WL, such as GIN (Xu et al., 2018), have a time complexity of $O(|E|)$. In contrast, 3-WL and existing GNNs with provable 3-WL expressive power are known to be computationally expensive, with a time complexity of at least $O(|V|^3)$ (Maron et al., 2019a). As a result, while these GNNs can offer strong expressive power, they are often impractical for real-world applications. The time complexities of our GPNNs fall between those of 1-WL and 3-WL, offering a balanced trade-off between computational efficiency and representational power. Specifically, the time complexities of GPNN * , GPNN $^\diamond$, and GPNN † are $O(|E| + q|E^\star|)$, $O(|E| + q|E^\diamond|)$, and $O(|E| + q|V|^2)$, respectively, where $q = \text{MAX}(\{|N_d(v)| \mid v \in V(G)\})$. Table 1 provides a detailed time complexity analysis of GPNNs, covering both vertex embedding and interaction embedding computations, and compares them with traditional GNNs and 3-WL.

	GIN	GCN	GPNN *	GPNN $^\diamond$	GPNN †	3-WL
VE	$O(E)$	$O(E)$	$O(E)$	$O(E)$	$O(E)$	-
IE	-	-	$O(q E^\star)$	$O(q E^\diamond)$	$O(q V ^2)$	$O(V ^3)$

Table 1: Time complexity analysis of different embedding computations, where **VE** refers to vertex embeddings and **IE** refers to interaction embeddings.

As shown in Table 1, GPNNs are more computationally efficient than 3-WL with a time complexity $O(|V|^3)$. This is due to two reasons. Firstly, real-world graphs are often sparse, and thus $|E^\star|$ and $|E^\diamond|$ are significantly smaller than $|V|^2$, i.e., $|E^\star| < |E^\diamond| \ll |V|^2$. Secondly, GPNNs only consider local neighbourhoods for learning interaction embeddings, i.e., vertices within a d -hop neighborhood, while 3-WL adopts a global neighbourhood, where the neighbours of each edge involve every vertex in the entire graph.

It is worth noting that the graph partitioning scheme used by GPNNs should be computationally efficient, i.e., in linear or polynomial time in terms of the size of an input graph. This

ensures that graph partitioning can be processed efficiently as a preprocessing step. In our experiments, we use a graph partitioning scheme with a time and space complexity of $O(|E|)$, which will be discussed in the next section.

7. Practical Choices of Partitioning Schemes

One might ask how to choose a graph partitioning scheme. In practice, there are many design options available. However, two important criteria must be met: *permutation invariance* and *computational efficiency*. To address these criteria, we first consider a graph partitioning scheme based on the k -core property (Malliaros et al., 2020), which is both permutation invariant and computationally efficient.

Definition 7.1 (k -Core Property). Let $\text{DEG}_S(v)$ denote the degree of vertex v in a subgraph S . A subgraph S has the *k -core property* on a graph G if S is the largest induced subgraph of G satisfying: $\forall v \in V(S) \text{ DEG}_S(v) \geq k$.

Let φ_j denote the j -core property and $\Phi_{\text{core}} = \{\phi_j\}_{j \in [0, k]}$ where $\phi_j = \varphi_j \wedge \neg\varphi_{j+1}$ satisfying the j -core property but not the $j+1$ -core property. The graph partitioning scheme $f_{\Phi_{\text{core}}}$ corresponds to the shell decomposition (Alvarez-Hamelin et al., 2005), which decomposes a graph G into a set of subgraphs, namely *shells*. Let $\phi \circ \psi$ denote the sequential composition of two properties ϕ and ψ . Then Φ_{core} can be further refined:

- $\Phi_{\text{core-degree}} = \{\phi'_j\}_{j \in [0, 2k]}$ where $\phi'_{2j-1} = \phi_j \circ \psi_j$, $\phi'_{2j} = \phi_j \circ \neg\psi_j$, and $\psi_j = \forall v \in V(S_j) \text{ DEG}_{S_j}(v) = j$.
- $\Phi_{\text{core-onion}} = \{\phi'_{ji}\}_{j \in [0, k]}$ where $\phi'_{ji} = \phi_j \circ \psi_j^1 \circ \dots \circ \psi_j^i$, and ψ_j^i refers to the i -th iteration to remove vertices with the lowest degree in the j -core subgraph.

Alternatively, we may consider graph partitioning schemes based on other properties such as vertex degrees. That is $\Phi_{\text{degree}} = \{\phi''_j\}_{j \in [0, k]}$ where ϕ''_j is defined as the set of vertices with a degree of j , and k is the maximum vertex degree in the graph. When computational resources are sufficient, more computationally demanding schemes can be considered, such as Φ_{triangle} where the partitioning is based on the number of triangles in which each vertex participates.

A question that might arise is how a partition colouring λ determined by such f_Φ relates to k -WL. The following theorem states that the expressive power of the partition colourings based on the k -core and degree properties are upper bounded by 1-WL.

Theorem 7.2. Let λ be a partition colouring based on f_Φ where $\Phi \in \{\Phi_{\text{core}}, \Phi_{\text{degree}}\}$. Then $G \equiv_\lambda H$ whenever $G \equiv_{1\text{-WL}} H$.

$\Phi_{\text{core-degree}}$ refines Φ_{core} by vertex degrees, while $\Phi_{\text{core-onion}}$ refines Φ_{core} based on degree correlations within each shell.

Methods	MUTAG	PTC-MR	PROTEINS	IMDB-B	BZR	COX2	ogbg-molhiv	ogbg-moltox21
¹ GIN	89.40 \pm 6.6	64.60 \pm 7.0	75.90 \pm 2.8	75.10 \pm 5.1	85.60 \pm 2.0	82.44 \pm 3.0	75.58 \pm 1.4	74.91 \pm 0.5
¹ GraphSNN	91.24 \pm 2.5	66.96 \pm 3.5	76.51 \pm 2.5	76.93 \pm 3.3	88.69 \pm 3.2	82.86 \pm 3.1	78.51 \pm 1.7	75.45 \pm 1.1
¹ ESAN	91.00 \pm 1.1	69.20 \pm 6.5	77.10 \pm 4.6	77.10 \pm 3.0	N/A	N/A	76.43 \pm 2.1	75.12 \pm 0.50
¹ CIN	92.70 \pm 6.1	68.20 \pm 5.6	77.00 \pm 4.3	75.60 \pm 3.7	N/A	N/A	80.94 \pm 0.6	N/A
¹ GIN-AK+	91.30 \pm 7.0	68.20 \pm 5.6	77.10 \pm 5.7	75.60 \pm 3.7	N/A	N/A	79.61 \pm 1.1	N/A
¹ KP-GIN	92.20 \pm 5.5	66.80 \pm 6.8	75.80 \pm 4.6	76.60 \pm 4.2	N/A	N/A	N/A	N/A
¹ PPGN	90.55 \pm 8.7	66.17 \pm 6.5	77.20 \pm 4.7	73.00 \pm 5.8	N/A	N/A	N/A	N/A
² GIN	92.80 \pm 5.9	65.60 \pm 6.5	78.80 \pm 4.1	78.10 \pm 3.5	91.05 \pm 3.4	88.87 \pm 2.3	75.58 \pm 1.4	74.91 \pm 0.5
² GraphSNN	94.70 \pm 1.9	70.58 \pm 3.1	78.42 \pm 2.7	78.51 \pm 2.8	91.12 \pm 3.0	86.28 \pm 3.3	78.51 \pm 1.7	75.45 \pm 1.1
² GIN-AK+	95.00 \pm 6.1	74.10 \pm 5.9	78.90 \pm 5.4	77.30 \pm 3.1	N/A	N/A	79.61 \pm 1.1	N/A
² KP-GIN	95.60 \pm 4.4	76.20 \pm 4.5	79.50 \pm 4.4	80.70 \pm 2.6	N/A	N/A	N/A	N/A
¹ $\lambda_{\text{core-degree}}$ -GPNN*	91.02 \pm 7.1	66.20 \pm 11.2	77.18 \pm 4.6	75.60 \pm 2.7	88.60 \pm 4.6	82.88 \pm 4.6	78.12 \pm 1.91	76.13 \pm 0.68
¹ $\lambda_{\text{core-degree}}$ -GPNN $^\diamond$	92.60 \pm 4.8	65.95 \pm 8.5	76.82 \pm 3.9	74.40 \pm 2.4	89.12 \pm 2.3	83.09 \pm 3.1	77.63 \pm 1.80	75.89 \pm 0.30
² $\lambda_{\text{core-degree}}$ -GPNN*	97.89 \pm 2.6	78.17 \pm 6.2	81.40 \pm 3.5	80.10 \pm 3.1	94.05 \pm 2.6	89.09 \pm 3.3	78.12 \pm 1.91	76.13 \pm 0.68
² $\lambda_{\text{core-degree}}$ -GPNN $^\diamond$	97.37 \pm 4.9	79.61 \pm 7.3	85.53 \pm 6.2	78.10 \pm 3.1	91.84 \pm 1.6	89.72 \pm 2.3	77.63 \pm 1.80	75.89 \pm 0.30

Table 2: Graph classification performance is reported as accuracy (%) for TU datasets and ROC (%) for OGB datasets. For the TU datasets, settings 1 and 2 correspond to the configurations used in Xu et al. (2018) and Feng et al. (2022), respectively. For OGB datasets, we employ the setup introduced by Hu et al. (2020). The best results for each setting are highlighted in **blue** for setting 1 and **black** for setting 2. Baseline results are sourced from Feng et al. (2022), Wijesinghe & Wang (2022), and Zhao et al. (2022a).

Theorem 7.2 applies to both schemes since the refinements are based on vertex degrees. However, it does not hold for Φ_{triangle} , which can distinguish graphs that are indistinguishable by 1-WL. The proof is included in the Appendix.

8. Experiments

We conduct experiments on three widely used benchmark tasks: graph classification, graph regression, and node classification. Due to the limited space, we present experimental results for graph regression tasks in the Appendix.

Datasets. We evaluate GPNNs on 15 benchmark datasets. For graph classification, we use six small-scale real-world datasets from TU Datasets (Morris et al., 2020a) and three large-scale molecular datasets from Open Graph Benchmark (OGB) (Hu et al., 2020). We also consider ZINC (Dwivedi et al., 2023) for graph regression, along with four widely used benchmark datasets for node classification (Sen et al., 2008; Craven et al., 2000).

Baselines. For graph classification, we choose GIN (Xu et al., 2018) as the base model for GPNNs and comparing them with GNNs beyond 1-WL: GIN, GraphSNN (Wijesinghe & Wang, 2022), GIN-AK+ (Zhao et al., 2022a), and KP-GIN (Feng et al., 2022), CIN (Bodnar et al., 2021), PPGN (Maron et al., 2019a), and ESAN (Bevilacqua et al., 2022). For node classification, we evaluate performance changes by incorporating our GPNN variants into standard GNNs, using GIN, GCN (Kipf & Welling, 2017), GAT (Velickovic et al., 2018), and GraphSAGE (Hamilton et al., 2017) as base models.

Detailed information for dataset statistics, experimental setups, and hyper-parameters is provided in the Appendix.

8.1. Results and Discussion

Exp-1. How do GPNNs perform for graph classification?

Table 2 reports the results. GPNN* and GPNN $^\diamond$ consistently outperform or match the baseline models. Compared to GPNN $^\diamond$, GPNN* handles fewer interactions but performs on par or exceeds the performance of GPNN $^\diamond$. This underscores that the presence of meaningful interactions are more paramount to learn graph structure than exhaustively exploring all interactions at the expense of computational efficiency. Unlike many existing models (e.g., (Bodnar et al., 2021)), GPNNs do not rely on hand-crafted, domain-specific structural information, such as cycles, which are often correlated with molecular datasets like OGB.

Exp-2. How do GPNNs perform for node classification?

Table 4 presents the results, demonstrating that GPNNs consistently enhance the performance of all standards methods across benchmark datasets, including both homophilic and heterophilic ones. This enhancement is attributed to GPNNs' ability to incorporate structural interactions as additional features into representations, which standard GNNs often overlook. This allows GPNNs to capture nuanced relationships between vertices, leading to enhanced performance compared to methods that rely solely on inter-interactions between vertices.

Exp-3: How does graph partitioning affect the learning of structural interactions? Table 5 shows the results for five partitioning schemes $\{\Phi_{\text{core}}, \Phi_{\text{core-degree}}$,

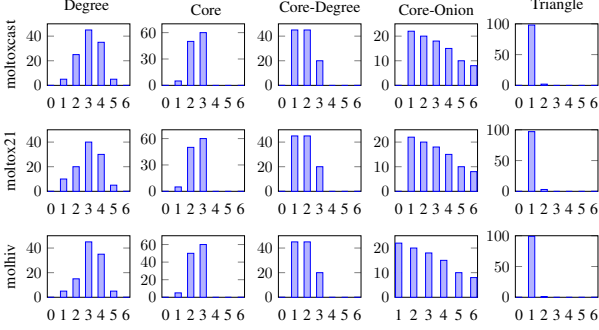


Figure 4: Node distribution percentage (y-axis) concerning partitions (x-axis) under different graph partitioning schemes for OGB Datasets.

$\Phi_{\text{core-onion}}, \Phi_{\text{degree}}, \Phi_{\text{triangle}}\}$. The vertex distribution across partitions for each partitioning scheme is illustrated in Figure 4. GPNNs outperform GIN across all partitioning schemes and datasets. $\Phi_{\text{core-degree}}$ and Φ_{degree} excel because they incorporate a significant amount of structural interactions into representations and also generate a sufficient number of partitions without imposing excessive computational burden. $\Phi_{\text{core-onion}}$ generates the most intra-interactions, but its high training complexity leads to subpar performance. Φ_{triangle} can distinguish graphs that 1-WL cannot, achieving strong performance even with fewer interactions.

Exp-4. How do different types of interactions affect performance? We examine how trivial and non-trivial partitioning schemes, as well as various types of interactions, impact GPNNs' performance. For the partitioning scheme, we use $\Phi_{\text{core-degree}}$, which balances interaction exploration with computational efficiency. Results are reported in Table 6. We can see that $\lambda_{\text{core-degree}}\text{-GPNN}^*$ consistently outperforms the corresponding $\lambda_{\perp}\text{-GPNN}^*$. All GPNNs show considerable improvements over GIN while $\lambda_{\perp}\text{-GPNN}^*$ has the closest results, empirically validating Proposition 5.1. Although GPNN^{\dagger} theoretically possess higher expressive power, its larger numbers of model parameters negatively affects model training and performance.

9. Conclusion, Limitations and Future Work

We introduced the notion of permutation-invariant graph partitioning to explore complex interactions among structural components. Building on this, we developed a novel GNN architecture to integrate structural interactions into graph representation learning. Our theoretical analysis shows how these interactions can enhance the expressive power of GNN models, establishing strong connections to the 1-WL and 3-WL tests, as well as their complexities. Empirical results validate the effectiveness of the proposed model.

In this work, permutation-invariant partitioning schemes

Methods	Cora	CiteSeer	Wisconsin	Texas
GIN	80.6 ± 0.4	73.8 ± 0.4	70.5 ± 1.6	61.6 ± 1.1
GPNN* _{GIN}	82.0 ± 1.4	74.8 ± 0.3	71.3 ± 1.7	62.3 ± 1.9
GPNN ^o _{GIN}	82.3 ± 0.9	74.2 ± 0.4	71.4 ± 1.5	61.5 ± 1.5
GCN	82.6 ± 1.5	78.1 ± 0.2	55.8 ± 19.5	53.1 ± 21.6
GPNN* _{GCN}	83.2 ± 1.5	78.8 ± 0.3	56.5 ± 17.7	51.8 ± 23.0
GPNN ^o _{GCN}	82.8 ± 1.7	78.6 ± 0.3	56.1 ± 18.2	57.7 ± 22.5
GAT	83.9 ± 0.8	77.7 ± 0.6	58.6 ± 1.6	62.0 ± 2.2
GPNN* _{GAT}	84.2 ± 0.8	78.1 ± 0.6	60.3 ± 2.5	64.3 ± 3.1
GPNN ^o _{GAT}	84.5 ± 0.4	77.8 ± 0.8	59.9 ± 2.5	64.4 ± 3.4
GraphSAGE	84.5 ± 0.3	77.9 ± 0.5	87.0 ± 1.7	81.6 ± 2.3
GPNN* _{GraphSAGE}	84.9 ± 0.3	78.2 ± 0.6	87.4 ± 1.2	79.5 ± 2.0
GPNN ^o _{GraphSAGE}	84.7 ± 0.5	78.1 ± 0.5	87.1 ± 1.6	82.0 ± 1.3

Table 4: Node classification accuracy (%). The best results are highlighted in **black**. The partitioning scheme Φ_{core} is used in the experiment.

Methods	ogbg-moltoxcast	ogbg-moltox21	ogbg-molhiv
GIN	63.41 ± 0.7	74.91 ± 0.5	75.58 ± 1.4
$\lambda_{\text{core}}\text{-GPNN}^*$	63.88 ± 0.8	75.34 ± 0.4	76.52 ± 1.1
$\lambda_{\text{core}}\text{-GPNN}^o$	63.59 ± 0.6	75.28 ± 0.5	75.91 ± 1.2
$\lambda_{\text{triangle}}\text{-GPNN}^*$	63.99 ± 0.4	75.20 ± 0.9	76.42 ± 1.2
$\lambda_{\text{triangle}}\text{-GPNN}^o$	63.41 ± 0.7	74.99 ± 0.6	75.92 ± 1.2
$\lambda_{\text{core-onion}}\text{-GPNN}^*$	62.91 ± 0.8	75.60 ± 0.5	76.57 ± 1.1
$\lambda_{\text{core-onion}}\text{-GPNN}^o$	61.86 ± 0.4	76.07 ± 0.5	77.03 ± 1.3
$\lambda_{\text{core-degree}}\text{-GPNN}^*$	64.70 ± 0.4	76.13 ± 0.7	78.12 ± 1.9
$\lambda_{\text{core-degree}}\text{-GPNN}^o$	64.48 ± 0.5	75.98 ± 0.4	77.70 ± 2.2
$\lambda_{\text{degree}}\text{-GPNN}^*$	65.28 ± 0.5	75.15 ± 0.7	78.98 ± 1.5
$\lambda_{\text{degree}}\text{-GPNN}^o$	64.81 ± 0.7	75.89 ± 0.3	77.63 ± 1.8

Table 5: Comparison of GPNNs in graph classification ROC (%) with five different graph partitioning schemes

Methods	MUTAG	PTC_MR	COX2	DHFR
GIN	92.80 ± 5.9	65.60 ± 6.5	88.87 ± 2.3	80.04 ± 4.9
$\lambda_{\perp}\text{-GPNN}^*$	94.74 ± 4.7	69.75 ± 5.1	87.37 ± 4.1	80.03 ± 4.0
$\lambda_{\perp}\text{-GPNN}^o$	96.32 ± 4.1	71.77 ± 4.3	89.37 ± 2.2	80.30 ± 3.0
$\lambda_{\perp}\text{-GPNN}^{\dagger}$	95.76 ± 3.2	71.43 ± 4.7	89.45 ± 2.1	78.97 ± 4.0
$\lambda_{\text{core-degree}}\text{-GPNN}^*$	97.89 ± 2.6	78.17 ± 6.2	89.09 ± 3.3	82.01 ± 2.3
$\lambda_{\text{core-degree}}\text{-GPNN}^o$	97.37 ± 4.9	79.61 ± 7.3	89.72 ± 2.3	82.15 ± 2.9
$\lambda_{\text{core-degree}}\text{-GPNN}^{\dagger}$	96.29 ± 3.4	80.05 ± 7.1	89.21 ± 2.8	80.16 ± 2.6

Table 6: Comparison of GPNN variants in graph classification accuracy (%) with different interaction types.

are not learned, and determining an effective scheme is largely application-dependent. From a theoretical perspective, however, it is an intriguing question how one might determine (or learn) optimal permutation-invariant partitioning schemes. In future work, we plan to explore data-driven methods to automatically identify partitioning schemes that preserve key structural properties for downstream graph tasks, independent of vertex ordering.

References

Abu-El-Haija, S., Perozzi, B., Kapoor, A., Alipourfard, N., Lerman, K., Harutyunyan, H., Ver Steeg, G., and Galstyan, A. Mixhop: Higher-order graph convolutional architectures via sparsified neighborhood mixing. In *international conference on machine learning*, 2019.

Alvarez-Hamelin, J., Dall'Asta, L., Barrat, A., and Vespignani, A. Large scale networks fingerprinting and visualization using the k-core decomposition. *Advances in neural information processing systems*, 2005.

Balcilar, M., Heroux, P., Gauzere, B., Vasseur, P., Adam, S., and Honeine, P. Breaking the limits of message passing graph neural networks. In *International Conference on Machine Learning*, 2021.

Barceló, P., Geerts, F., Reutter, J., and Ryschkov, M. Graph neural networks with local graph parameters. *Advances in Neural Information Processing Systems*, 34:25280–25293, 2021.

Beaini, D., Passaro, S., Ltourneau, V., Hamilton, W., Corso, G., and Lio, P. Directional graph networks. In *International Conference on Machine Learning*, 2021.

Bevilacqua, B., Frasca, F., Lim, D., Srinivasan, B., Cai, C., Balamurugan, G., Bronstein, M. M., and Maron, H. Equivariant subgraph aggregation networks. *International Conference on Learning Representations*, 2022.

Bodnar, C., Frasca, F., Otter, N., Wang, Y., Lio, P., Montufar, G. F., and Bronstein, M. Weisfeiler and lehman go cellular: Cw networks. *Advances in Neural Information Processing Systems*, 2021.

Bouritsas, G., Frasca, F., Zafeiriou, S. P., and Bronstein, M. Improving graph neural network expressivity via subgraph isomorphism counting. *IEEE Transactions on Pattern Analysis and Machine Intelligence*, 2022.

Cai, J.-Y., Furer, M., and Immerman, N. An optimal lower bound on the number of variables for graph identification. *Combinatorica*, 12(4):389–410, 1992.

Chen, Z., Chen, L., Villar, S., and Bruna, J. Can graph neural networks count substructures? *Advances in neural information processing systems*, 2020.

Chiang, W.-L., Liu, X., Si, S., Li, Y., Bengio, S., and Hsieh, C.-J. Cluster-gcn: An efficient algorithm for training deep and large graph convolutional networks. In *Proceedings of the 25th ACM SIGKDD international conference on knowledge discovery & data mining*, 2019.

Cotta, L., Morris, C., and Ribeiro, B. Reconstruction for powerful graph representations. *Advances in Neural Information Processing Systems*, 2021.

Craven, M., DiPasquo, D., Freitag, D., McCallum, A., Mitchell, T., Nigam, K., and Slattery, S. Learning to construct knowledge bases from the world wide web. *Artificial intelligence*, 118(1-2):69–113, 2000.

Dwivedi, V. P., Joshi, C. K., Luu, A. T., Laurent, T., Bengio, Y., and Bresson, X. Benchmarking graph neural networks. *Journal of Machine Learning Research*, 24(43):1–48, 2023.

Feng, J., Chen, Y., Li, F., Sarkar, A., and Zhang, M. How powerful are k-hop message passing graph neural networks. *Advances in Neural Information Processing Systems*, 2022.

Frasca, F., Bevilacqua, B., Bronstein, M., and Maron, H. Understanding and extending subgraph gnns by rethinking their symmetries. *Advances in Neural Information Processing Systems*, 35:31376–31390, 2022.

Gaunt, A., Tarlow, D., Brockschmidt, M., Urtasun, R., Liao, R., and Zemel, R. Graph partition neural networks for semi-supervised classification. 2018.

Gilmer, J., Schoenholz, S. S., Riley, P. F., Vinyals, O., and Dahl, G. E. Neural message passing for quantum chemistry. In *International conference on machine learning*, pp. 1263–1272. PMLR, 2017.

Hamilton, W., Ying, Z., and Leskovec, J. Inductive representation learning on large graphs. *Advances in neural information processing systems*, 2017.

He, J., Huang, Z., Wang, N., and Zhang, Z. Learnable graph matching: Incorporating graph partitioning with deep feature learning for multiple object tracking. In *Proceedings of the IEEE/CVF conference on computer vision and pattern recognition*, pp. 5299–5309, 2021.

Horn, M., De Brouwer, E., Moor, M., Moreau, Y., Rieck, B., and Borgwardt, K. Topological graph neural networks. *International Conference on Learning Representations*, 2022.

Hu, W., Fey, M., Zitnik, M., Dong, Y., Ren, H., Liu, B., Catasta, M., and Leskovec, J. Open graph benchmark: Datasets for machine learning on graphs. *Advances in neural information processing systems*, 2020.

Huang, Y., Peng, X., Ma, J., and Zhang, M. Boosting the cycle counting power of graph neural networks with i^2 -gnns. *International Conference on Learning Representations*, 2023.

Irwin, J. J., Sterling, T., Mysinger, M. M., Bolstad, E. S., and Coleman, R. G. Zinc: a free tool to discover chemistry for biology. *Journal of chemical information and modeling*, 52(7):1757–1768, 2012.

Jin, E., Bronstein, M. M., Ceylan, I. I., and Lanzinger, M. Homomorphism counts for graph neural networks: All about that basis. In *Forty-first International Conference on Machine Learning*, 2024.

Kingma, D. Adam: a method for stochastic optimization. In *International Conference on Learning Representations*, 2015.

Kipf, T. N. and Welling, M. Semi-supervised classification with graph convolutional networks. *International Conference on Learning Representations*, 2017.

Lin, W. Large-scale network embedding in apache spark. In *Proceedings of the 27th ACM SIGKDD Conference on Knowledge Discovery & Data Mining*, pp. 3271–3279, 2021.

Malliaros, F. D., Giatsidis, C., Papadopoulos, A. N., and Vazirgiannis, M. The core decomposition of networks: Theory, algorithms and applications. *The VLDB Journal*, 29(1):61–92, 2020.

Maron, H., Ben-Hamu, H., Serviansky, H., and Lipman, Y. Provably powerful graph networks. *Advances in neural information processing systems*, 2019a.

Maron, H., Fetaya, E., Segol, N., and Lipman, Y. On the universality of invariant networks. In *International conference on machine learning*, 2019b.

McKay, B. D. and Piperno, A. Practical graph isomorphism, ii. *Journal of symbolic computation*, 60:94–112, 2014.

Miao, X., Gurel, N. M., Zhang, W., Han, Z., Li, B., Min, W., Rao, S. X., Ren, H., Shan, Y., Shao, Y., et al. Degnn: Improving graph neural networks with graph decomposition. In *Proceedings of the 27th ACM SIGKDD Conference on Knowledge Discovery & Data Mining*, 2021.

Morris, C., Ritzert, M., Fey, M., Hamilton, W. L., Lenssen, J. E., Rattan, G., and Grohe, M. Weisfeiler and leman go neural: Higher-order graph neural networks. In *Proceedings of the AAAI conference on artificial intelligence*, 2019.

Morris, C., Kriege, N. M., Bause, F., Kersting, K., Mutzel, P., and Neumann, M. Tudataset: A collection of benchmark datasets for learning with graphs. *ICML workshop 'Graph Representation Learning and Beyond'*, 2020a.

Morris, C., Rattan, G., and Mutzel, P. Weisfeiler and leman go sparse: Towards scalable higher-order graph embeddings. *Advances in Neural Information Processing Systems*, 2020b.

Mu, Z., Tang, S., Zong, C., Yu, D., and Zhuang, Y. Graph neural networks meet with distributed graph partitioners and reconciliations. *Neurocomputing*, 518:408–417, 2023.

Nikolentzos, G., Dasoulas, G., and Vazirgiannis, M. k-hop graph neural networks. *Neural Networks*, 130:195–205, 2020.

Pei, H., Wei, B., Chang, K. C.-C., Lei, Y., and Yang, B. Geom-gcn: Geometric graph convolutional networks. *International Conference on Learning Representations*, 2020.

Sato, R. A survey on the expressive power of graph neural networks. *arXiv preprint arXiv:2003.04078*, 2020.

Sen, P., Namata, G., Bilgic, M., Getoor, L., Galligher, B., and Eliassi-Rad, T. Collective classification in network data. *AI magazine*, 29(3):93–93, 2008.

Smith, K. M. On neighbourhood degree sequences of complex networks. *Scientific reports*, 9(1):8340, 2019.

Velickovic, P., Cucurull, G., Casanova, A., Romero, A., Lio, P., and Bengio, Y. Graph attention networks. In *International Conference on Learning Representations*, 2018.

Wan, X., Xu, K., Liao, X., Jin, Y., Chen, K., and Jin, X. Scalable and efficient full-graph gnn training for large graphs. *Proceedings of the ACM on Management of Data*, 1(2):1–23, 2023.

Wang, X. and Zhang, M. Glass: Gnn with labeling tricks for subgraph representation learning. In *International Conference on Learning Representations*, 2022.

Wang, Z., Cao, Q., Shen, H., Bingbing, X., Zhang, M., and Cheng, X. Towards efficient and expressive gnns for graph classification via subgraph-aware weisfeiler-lehman. In *The First Learning on Graphs Conference*, 2022.

Weisfeiler, B. and Leman, A. The reduction of a graph to canonical form and the algebra which appears therein. *nti, Series*, 2(9):12–16, 1968a.

Weisfeiler, B. and Leman, A. The reduction of a graph to canonical form and the algebra which appears therein. *nti, Series*, 2(9):12–16, 1968b.

Wijesinghe, A. and Wang, Q. A new perspective on how graph neural networks go beyond weisfeiler-lehman? In *International Conference on Learning Representations*, 2022.

Xu, H., Chen, R., Bai, Y., Feng, J., Duan, Z., Luo, K., Sun, Y., and Wang, W. Hierarchical and fast graph similarity computation via graph coarsening and deep graph learning. *arXiv preprint arXiv:2005.07115*, 2020.

Xu, H., Duan, Z., Wang, Y., Feng, J., Chen, R., Zhang, Q., and Xu, Z. Graph partitioning and graph neural network based hierarchical graph matching for graph similarity computation. *Neurocomputing*, 439:348–362, 2021.

Xu, J., Zhang, A., Bian, Q., Dwivedi, V. P., and Ke, Y. Union subgraph neural networks. In *Proceedings of the AAAI Conference on Artificial Intelligence*, volume 38, pp. 16173–16183, 2024.

Xu, K., Hu, W., Leskovec, J., and Jegelka, S. How powerful are graph neural networks? In *International Conference on Learning Representations*, 2018.

Yang, S., Zhang, M., Dong, W., and Li, D. Betty: Enabling large-scale gnn training with batch-level graph partitioning. In *Proceedings of the 28th ACM International Conference on Architectural Support for Programming Languages and Operating Systems, Volume 2*, pp. 103–117, 2023.

Ye, Y., Lian, X., and Chen, M. Efficient exact subgraph matching via gnn-based path dominance embedding.

You, J., Gomes-Selman, J. M., Ying, R., and Leskovec, J. Identity-aware graph neural networks. In *Proceedings of the AAAI conference on artificial intelligence*, 2021.

Zeng, D., Liu, W., Chen, W., Zhou, L., Zhang, M., and Qu, H. Substructure aware graph neural networks. In *Proceedings of the AAAI Conference on Artificial Intelligence*, volume 37, pp. 11129–11137, 2023.

Zhang, B., Fan, C., Liu, S., Huang, K., Zhao, X., Huang, J., and Liu, Z. The expressive power of graph neural networks: A survey. *IEEE Transactions on Knowledge and Data Engineering*, 2024a.

Zhang, B., Gai, J., Du, Y., Ye, Q., He, D., and Wang, L. Beyond weisfeiler-lehman: A quantitative framework for gnn expressiveness. In *The Twelfth International Conference on Learning Representations*, 2024b.

Zhang, M. and Li, P. Nested graph neural networks. *Advances in Neural Information Processing Systems*, 34: 15734–15747, 2021.

Zhao, L., Jin, W., Akoglu, L., and Shah, N. From stars to subgraphs: Uplifting any gnn with local structure awareness. *International Conference on Learning Representations*, 2022a.

Zhao, L., Shah, N., and Akoglu, L. A practical, progressively-expressive gnn. *Advances in Neural Information Processing Systems*, 2022b.

Appendix

A. Model Architecture

In this section, we describe the implementation details of our GPNN architecture. Let $\beta_v^{(0)} = \lambda_V(v)$, $\gamma_v^{(0)} = \lambda_V(v)$ and $\alpha_{vu}^{(0)} = \lambda_E(v, u)$. Equations 1 and 2 for the vertex and interaction embeddings are implemented as follows:

$$\begin{aligned} \beta_v^{(\ell+1)} &= \text{MLP}_\theta^{(\ell+1)} \left(\left(1 + \epsilon^{(\ell+1)} \right) \gamma_v^{(\ell)} \right. \\ &\quad \left. + \sum_{u \in N(v)} \gamma_u^{(\ell)} \right); \end{aligned} \quad (5)$$

$$\begin{aligned} \alpha_{vu}^{(\ell+1)} &= \text{MLP}_\psi^{(\ell+1)} \left(\left(1 + \mu^{(\ell+1)} \right) \alpha_{vu}^{(\ell)} \right. \\ &\quad \left. + \sum_{w \in N_d(v)} \left(\alpha_{vw}^{(\ell)} + \alpha_{vw}^{(\ell)} \right) \right). \end{aligned} \quad (6)$$

Here, $\beta_v^{(\ell+1)} \in \mathbb{R}^f$ is a vertex embedding; $\alpha_{vu}^{(\ell+1)} \in \mathbb{R}^f$ is an interaction embedding; $\gamma_v^{(\ell+1)} \in \mathbb{R}^f$ is an embedding that combines vertex embeddings and the corresponding interaction embeddings from the colored neighborhood of vertex v ; $\mu^{(\ell+1)}$ and $\epsilon^{(\ell+1)}$ are learnable scalar parameters; $\text{MLP}_\theta^{(\ell+1)}(\cdot)$ and $\text{MLP}_\psi^{(\ell+1)}(\cdot)$ are multi-layer perceptron (MLP) functions, parameterized by θ and ψ , respectively.

The embedding $\gamma_{v,j}^{(\ell+1)}$ for each $j \in [1, k]$ is calculated as,

$$\gamma_{v,j}^{(\ell+1)} = \omega_j \left(\sum_{u \in N_d^j(v)} \left(\beta_u^{(\ell+1)} \parallel \alpha_{vu}^{(\ell+1)} \parallel p_j \right) W_j \right). \quad (7)$$

The combined embedding w.r.t. the whole neighborhood of vertex v is defined as

$$\gamma_v^{(\ell+1)} = \left(\gamma_{v,1}^{(\ell+1)} + \dots + \gamma_{v,k}^{(\ell+1)} \right). \quad (8)$$

For any $j \in [1, k]$, $\gamma_{v,j}^{(\ell+1)}$ is the vertex embedding of v learned at the $(\ell+1)$ -th iteration concerning a neighboring vertex subset $N_d^j(v)$; $p_j \in \mathbb{R}^{1 \times k}$ is a one-hot vector in which values are all zero except one at the j -th position; $W_j \in \mathbb{R}^{(2f+k) \times f}$ is a learnable linear transformation matrix; ω_j is a learnable scalar parameter. It is worth noting that p_j is critical for preserving the injectivity of Equation 3

in GPNN.

When GPNN is used as a plug-in, $\gamma^{(\ell+1)}$ can be concatenated with the corresponding vertex embedding h_v^{gnn} generated by a chosen GNN as follows:

$$h_v = \text{CONCAT} \left(h_v^{gnn}, \gamma^{(\ell+1)} \right) \quad (9)$$

Finally, we append a feature vector related to the number of connected components, provided by the graph partitioning scheme, to h_v to enhance the representations.

B. Proofs

In the following we provide the proofs to the propositions, lemmas, and theorems presented in Section 5. Without loss of generality, we assume that the functions $\text{AGG}(\cdot)$, $\text{CMB}(\cdot)$ and $\text{UPD}(\cdot)$ used in GPNN are injective and there are also sufficiently many layers in GPNN.

Theorem 3.5. *Fix a graph partitioning scheme. We have:*

(a) *If $G \simeq G'$, then $G \xrightarrow{II} G'$, but not vice versa;* (b) *If $G \xrightarrow{II} G'$, then $G \xrightarrow{PI} G'$, but not vice versa.*

Proof. Suppose that the graph partitioning scheme is f_Φ . We first prove one direction of Statement (a), i.e., if $G \simeq G'$, then $G \xrightarrow{II} G'$. From the definition of graph isomorphism, we know that if $G \simeq G'$, then there is a bijective mapping $f : V(G) \rightarrow V(G')$ such that for any $(u, v) \in E(G)$, $(f(u), f(v)) \in E(G')$, and vice versa. By Definition 3.2, we know that if $G \xrightarrow{PI} G'$, then there exists a bijective mapping $g : f_\Phi(G) \rightarrow f_\Phi(G')$ such that $g(S_i) \simeq S'_i$ for every $i \in [1, k]$. Thus, if $G \simeq G'$, we know that the same bijective mapping from graph isomorphism $f : V(S_i) \rightarrow V(S'_i)$ satisfies that for any $(u, v) \in E(S_i)$, $(f(u), f(v)) \in E(S'_i)$ for any $i \in [1, k]$. Then, we consider the boundary subgraphs $B(G) = (\mathcal{V}, \mathcal{E})$ and $B(G') = (\mathcal{V}', \mathcal{E}')$. By Definition 3.4, it requires to show a bijective function $g : B(G) \rightarrow B(G')$ such that $(v, u) \in \mathcal{E}$ iff $(g(v), g(u)) \in \mathcal{E}'$. This can also be satisfied by f where $f : \mathcal{V} \rightarrow \mathcal{V}'$ such that for any $(u, v) \in \mathcal{E}$, $(f(u), f(v)) \in \mathcal{E}'$. Therefore, such a bijective mapping f of graph isomorphism satisfies both of the conditions of interaction-isomorphism. This direction is proven. However, the converse direction of Statement (a) does not hold. The pair of graphs shown in Figure 2(a) is interaction-isomorphic, but not isomorphic.

For Statement (b), the first direction (i.e., if $G \xrightarrow{II} G'$, then $G \xrightarrow{PI} G'$) can easily follow from the definition of interaction-isomorphism. The converse do not hold, which can be proven by the pair of graphs shown in Figure 2(b).

The proof is complete. \square

Before proving the next theorem, we recall 2-FWL test (Weisfeiler & Leman, 1968a) which has been shown to be logically equivalent to 3-WL test (Maron et al., 2019a). 2-FWL test initially provides a color $C^0(v, u)$ for each pair of vertices $v, u \in V(G)$, defined as follows.

$$C^0(v, u) = \begin{cases} c_{self} & u = v \\ c_{interaction} & (u, v) \in E(G) \\ c_{non-interaction} & (u, v) \notin E(G) \end{cases}$$

Here, c_{self} , $c_{interaction}$ and $c_{non-interaction}$ are initial colours. Then the iterative coloring process of 2-FWL is defined by:

$$C^{(i+1)}(v, u) = \sigma \left(C^{(i)}(v, u), \right. \\ \left. \{(C^{(i)}(v, w), C^{(i)}(u, w)) \mid w \in V(G)\} \right). \quad (10)$$

Note that $\sigma(\cdot)$ is an injective hashing function. The expressive power of 2-FWL is known to be strictly higher than 1-WL test and 2-WL test (Balciar et al., 2021).

Proposition 5.1. *The following hold: (1) $\lambda_{\perp}\text{-GPNN}^* \equiv 1\text{-WL}$; (2) $\lambda_{\perp}\text{-GPNN}^* \sqsubseteq \lambda_{\perp}\text{-GPNN}^{\diamond} \sqsubseteq \lambda_{\perp}\text{-GPNN}^{\dagger}$; (3) $\lambda_{\perp}\text{-GPNN}^{\dagger} \sqsubseteq 3\text{-WL}$.*

Proof. We first prove Statement (1) $\lambda_{\perp}\text{-GPNN}^* \equiv 1\text{-WL}$. According to the model design, $\lambda_{\perp}\text{-GPNN}^*$ starts with Equation (1). Since λ_{\perp} is trivial, $E^* = \emptyset$, meaning that all vertices are initially assigned the same colour. In Equation (1), a vertex embedding is updated based on its previous embedding and the embeddings of its direct neighbours. This implies that for, without any iteration embedding, for any iteration of Equation (1) has expressive power upper bounded by 1-WL, as demonstrated in Theorem 3 of Xu et al. (2018). $\lambda_{\perp}\text{-GPNN}^*$ does not account for any structural interactions. Therefore, Equation (2) does not contribute additional expressivity. Given that Equation (3) is an injective combination of Equation (1) and Equation (2) from the neighbours of each vertex and the vertex itself, the expressive power of the final embedding in any iteration is also upper-bounded by 1-WL. This completes the first part of the proof.

We then prove Statement (2) $\lambda_{\perp}\text{-GPNN}^* \sqsubseteq \lambda_{\perp}\text{-GPNN}^{\diamond} \sqsubseteq \lambda_{\perp}\text{-GPNN}^{\dagger}$. Given that $E^* \subseteq E^{\diamond} \subseteq E^{\dagger}$, it is trivial to see that $\lambda\text{-GPNN}^* \sqsubseteq \lambda\text{-GPNN}^{\diamond} \sqsubseteq \lambda\text{-GPNN}^{\dagger}$.

Finally, we prove Statement (3) $\lambda_{\perp}\text{-GPNN}^{\dagger} \sqsubseteq 3\text{-WL}$. When accounting for all of inter-interactions, intra-interactions and non-interactions in a graph, the expressive power of Equation (2) is upper-bounded by 2-FWL (i.e., equivalent to 3-WL in terms of their ability in distinguishing non-isomorphic graphs). Since λ is trivial, the initial

vertex colours by λ_{\perp} do not provide any additional power beyond that of 1-WL. Therefore, for any iteration, the final embeddings generated by any GPNN variant are upper bounded by 3-WL, meaning that $\lambda\text{-GPNN}^{\dagger} \sqsubseteq 3\text{-WL}$. \square

Theorem 5.2. *Let λ_1 and λ_2 be two partition colourings with $\lambda_1 \sqsupseteq \lambda_2$. Then $\lambda_1\text{-GPNN}^{\delta} \sqsubseteq \lambda_2\text{-GPNN}^{\delta}$ for any $\delta \in \{\star, \diamond, \dagger\}$.*

Proof. By the definition of $\lambda\text{-GPNN}^{\delta}$, GPNN starts with a graph in which vertices are coloured by λ . Since $\lambda_1 \sqsupseteq \lambda_2$, we know that, for any two vertices $\{v, u\} \subseteq V(G)$, if v and u are assigned with the same colour by λ_1 , then they must be assigned with the same colour by λ_2 ; the converse does not necessarily hold. Then, by the definition of GPNN in terms of Equations 1, 2, and 3, we know that if two vertices $\{v, u\} \subseteq V(G)$ are assigned with different colours by λ , then they would always have different colours after applying $\lambda\text{-GPNN}^{\delta}$ with any number of layers. That is, $\lambda\text{-GPNN}^{\delta}$ always *refines* a partitioning colouring λ . Since the same equations (Equations 1, 2, and 3) are applied by $\lambda_1\text{-GPNN}^{\delta}$ and $\lambda_2\text{-GPNN}^{\delta}$ on vertices in G , which only differ in partitioning colourings, and also the functions $\text{AGG}(\cdot)$, $\text{CMB}(\cdot)$ and $\text{UPD}(\cdot)$ used in GPNN are injective, any two vertices $v, u \in V(G)$ must have different colours by applying $\lambda_1\text{-GPNN}^{\delta}$ whenever they have different colours by applying $\lambda_2\text{-GPNN}^{\delta}$, but not vice versa. \square

Theorem 5.3. *Let λ be a partition colouring satisfying $\lambda \sqsubseteq k\text{-WL}$ or $\lambda \sqsupseteq k\text{-WL}$ for some $k \in \mathbb{N}$. Then $\max(\lambda, 1\text{-WL}) \sqsubseteq \lambda\text{-GPNN}^{\delta}$ and $\lambda\text{-GPNN}^{\delta} \sqsubseteq \max(\lambda, 3\text{-WL})$ for any $\delta \in \{\star, \diamond, \dagger\}$.*

Proof. From Proposition 5.1, we know that $\lambda_{\perp}\text{-GPNN}^* \equiv 1\text{-WL}$. By Theorem 5.2, for any non-trivial λ , $\lambda\text{-GPNN}^*$ is at least as expressive as $\lambda_{\perp}\text{-GPNN}^*$. Hence, we can deduce that $\lambda\text{-GPNN}^*$ is at least lower bounded by 1-WL. When λ is strictly more expressive than 1-WL, any iteration of GPNN will be strictly more expressive than the corresponding 1-WL iteration as Equation (1) and Equation (3) together can only further refine initial vertex colours. In this case, $\lambda\text{-GPNN}^*$ is lower bounded by λ . Therefore, we can conclude that, for any λ , $\max(\lambda, 1\text{-WL}) \sqsubseteq \lambda\text{-GPNN}^*$. Given that $E^* \subseteq E^{\diamond} \subseteq E^{\dagger}$, we can deduce that $\lambda\text{-GPNN}^* \sqsubseteq \lambda\text{-GPNN}^{\diamond} \sqsubseteq \lambda\text{-GPNN}^{\dagger}$. Therefore, this relationship also holds for the other two GPNN variants, as they are at least as expressive as the corresponding $\lambda\text{-GPNN}^*$.

From Proposition 5.1, we also know that $\lambda_{\perp}\text{-GPNN}^{\delta}$ is upper bounded by 3-WL. Additionally, if $\lambda \sqsubseteq 3\text{-WL}$, then for any non-trivial λ , $\lambda\text{-GPNN}^{\delta}$ is also upper bounded by 3-WL. This is because initial vertex coloring is upper bounded by 3-WL, and any interaction learning in GPNNs is similarly constrained by 3-WL, leading to final embeddings that are upper bounded by 3-WL. When λ is strictly more powerful

than 3-WL, GPNN is as expressive as λ , since no iteration of GPNN can further refine the color beyond λ . Therefore, for any λ , we have $\lambda\text{-GPNN}^\dagger \sqsubseteq \max(\lambda, 3\text{-WL})$. \square

Lemma 5.1. *When $\lambda \sqsubset 3\text{-WL}$, $\lambda\text{-GPNN}^\dagger \sqsupseteq \lambda\text{-GPNN}^\diamond \sqsupseteq \lambda\text{-GPNN}^*$. When $\lambda \sqsupseteq 3\text{-WL}$, $\lambda\text{-GPNN}^\dagger \equiv \lambda\text{-GPNN}^\diamond \equiv \lambda\text{-GPNN}^*$.*

Proof. First, we consider the case where $\lambda \sqsubset 3\text{-WL}$. Since $E^* \subseteq E^\diamond \subseteq E^\dagger$, for any λ , we can derive the following: $\lambda\text{-GPNN}^* \sqsubseteq \lambda\text{-GPNN}^\diamond \sqsubseteq \lambda\text{-GPNN}^\dagger$.

Next, we consider the case where $\lambda \sqsupseteq 3\text{-WL}$. In this case, by $\max(\lambda, 1\text{-WL}) \sqsubseteq \lambda\text{-GPNN}^\delta$, as stated in Theorem 5.3, we know that the expressive power of $\lambda\text{-GPNN}^\delta$ is lower-bounded by λ . Similarly, by $\lambda\text{-GPNN}^\dagger \sqsubseteq \max(\lambda, 3\text{-WL})$ from Theorem 5.3, we know that the expressive power of $\lambda\text{-GPNN}^\dagger$ is also upper-bounded by λ . Therefore, all GPNN variants ($\lambda\text{-GPNN}^\delta$) will have the same expressive power, determined by the initial partition coloring λ , regardless of the interaction types $\delta \in \{\star, \diamond, \dagger\}$ considered. Thus, $\lambda\text{-GPNN}^\dagger \equiv \lambda\text{-GPNN}^\diamond \equiv \lambda\text{-GPNN}^*$ holds. \square

Theorem 5.4. *For any partition colouring λ , $\lambda\text{-GPNN}^\dagger \sqsupseteq \lambda\text{-GPNN}^\diamond \sqsupseteq \lambda\text{-GPNN}^*$.*

Proof. Given that λ determines the initial vertex colouring in GPNNs, any pair of graphs distinguished by λ will also be distinguished by any GPNN variant. Additionally, since $E^* \subseteq E^\diamond \subseteq E^\dagger$, it follows that for any λ , $\text{GPNN}^* \sqsubseteq \text{GPNN}^\diamond \sqsubseteq \text{GPNN}^\dagger$. This completes the proof. \square

Theorem 7.2. *Let λ be a partition colouring based on f_Φ where $\Phi \in \{\Phi_{\text{core}}, \Phi_{\text{degree}}\}$. Then $G \equiv_\lambda H$ whenever $G \equiv_{1\text{-WL}} H$.*

Proof. We first prove the theorem for Φ_{core} . Let $\lambda_{1\text{-WL}}$ and λ_{core} be two partition colorings generated by 1-WL and core decomposition based on the k-core property (Definition 7.1), respectively. 1-WL is a coloring algorithm that iteratively captures the neighborhood degree sequence of each vertex in a graph (Smith, 2019). If $\lambda_{1\text{-WL}}(u) = \lambda_{1\text{-WL}}(v)$, then the vertices u and v must have identical neighborhood degree sequence. Core decomposition is an iterative peeling algorithm that, given an input graph G , the peeling process starts from vertices of the lowest degree in the graph G . Assume that there are two vertices u and v s.t. $\lambda_{1\text{-WL}}(u) = \lambda_{1\text{-WL}}(v)$ and $\lambda_{\text{core}}(u) \neq \lambda_{\text{core}}(v)$. Since $\lambda_{\text{core}}(u) \neq \lambda_{\text{core}}(v)$, u and v must appear in different peeling iterations; otherwise, they would have the same color from the core decomposition. Let P_u and P_v be two sets containing all vertices removed in the peeling iterations before u and v are removed by the core decomposition

algorithm, respectively. Since $\lambda_{\text{core}}(u)$ and $\lambda_{\text{core}}(v)$ are different, K-shell numbers (Alvarez-Hamelin et al., 2005) of u and v must be distinct. Without loss of generality, we assume that the K-shell value of v is larger than the K-shell value of u . Then, P_u must be a proper subset of P_v (i.e. $P_u \subset P_v$). In other words, P_u cannot be the same as P_v . Thus, P_u and P_v should have different degree sequences. Since, u and v have different degree sequences around them, their coloring received from 1-WL should be different. This contradicts the above assumption. Therefore, $\lambda_{1\text{-WL}}(u) = \lambda_{1\text{-WL}}(v) \implies \lambda_{\text{core}}(u) = \lambda_{\text{core}}(v)$. This also implies that if the colors of any two nodes in two graphs G and H are the same by 1-WL, then their node colors by core decomposition must also be the same. Therefore, under an injective graph readout function, if $G \equiv_{1\text{-WL}} H$, then $G \equiv_{\text{core}} H$.

Then, we prove the theorem for Φ_{degree} . Let $\lambda_{1\text{-WL}}$ and λ_{degree} be two partition colourings generated by 1-WL and degrees of vertices, respectively. Since the 1st iteration of 1-WL captures the 1-hop neighborhood degree sequence of each vertex, the colouring produced by the 1st iteration of 1-WL must be equivalent to the colouring of λ_{degree} . Further iterations of 1-WL would only refine the colours of vertices. This implies that if the colours of any two vertices in two graphs G and H are the same by 1-WL, then their vertex colours by λ_{degree} must also be the same, i.e. $\forall u, v \in V(G), \lambda_{1\text{-WL}}(u) = \lambda_{1\text{-WL}}(v) \implies \lambda_{\text{degree}}(u) = \lambda_{\text{degree}}(v)$, although the converse does not generally hold. Therefore, under an injective graph readout function, if $G \equiv_{1\text{-WL}} H$, then $G \equiv_{\text{degree}} H$. \square

C. Supplementary Experimental Details

In this section, we describe the statistics of the benchmark datasets, model hyper-parameters, and computational resources related to our experiments.

C.1. Benchmark Dataset Statistics

Table 7 and Table 8, provide a summary of statistics for datasets that we have considered in all our experiments. Table 7 consists of the dataset statistics for graph classification and graph regression, whereas Table 8 contains the dataset statistics for node classification.

Datasets	# Nodes	# Edges	# Features	# Classes
Cora	2708	5278	1433	7
CiteSeer	3327	4552	3703	6
Wisconsin	251	466	1703	5
Texas	183	279	1703	5

Table 8: Dataset statistics for node classification

Datasets	Task Type	# Graphs	Avg #Nodes	Avg #Edges	# Classes
MUTAG	Graph Classification	188	17.93	19.79	2
PTC_MR	Graph Classification	344	14.29	14.69	2
BZR	Graph Classification	405	35.75	38.36	2
COX2	Graph Classification	467	41.22	43.45	2
DHFR	Graph Classification	756	42.43	44.54	2
IMDB-B	Graph Classification	1,000	19.77	96.53	2
PROTEINS	Graph Classification	1,113	39.06	72.82	2
ogbg-moltox21	Graph Classification	7,831	18.6	19.3	2
ogbg-moltocast	Graph Classification	8,576	18.8	19.3	2
ogbg-molhiv	Graph Classification	41,127	25.5	27.5	2
ZINC	Graph Regression	12,000	23.1	49.8	1

Table 7: Dataset statistics for graph classification and regression

C.2. Experimental Setups

In graph classification, we adopt the setup outlined by Hu et al. (2020) for the OGB datasets. For TU datasets, we present results under two distinct configurations: Setting 1 as described by Xu et al. (2018) and Setting 2 by Feng et al. (2022). In the first setting, we report the average test accuracy across 10 folds and the standard deviation for the epoch with the highest mean accuracy. In the second setting, we provide the mean and standard deviation of the best accuracy across all test folds. For node classification, we follow the setup suggested in Pei et al. (2020), where vertices in the datasets are randomly split into 60%, 20%, and 20% for training, validation, and testing, respectively.

C.3. Hyper-parameters

In our experiments, the hyper-parameters of GPNN are searched in the following ranges: the number of layers is within $\{1, 2, 3, 4, 5\}$, $d \in \{1, 2, 3, 4, 5\}$, dropout $\in \{0.0, 0.1, 0.2, 0.5, 0.6\}$, learning rate $\in \{0.009, 0.01\}$, batch size $\in \{32, 64, 128\}$, hidden units $\in \{32, 64, 100\}$, and the number of epochs $\in \{100, 200, 300, 500\}$. We use the Adam algorithm (Kingma, 2015) as our optimizer. For ZINC and OGB datasets, the initial learning rate decays with a factor of 0.5 after every 10 epochs. We do not use any learning rate decay technique for TU datasets.

C.4. Graph Regression Tasks

We provide additional experiments related to graph regression and discuss the impact of different graph partition schemes on the performance of GPNNs. In this experiments, we follow the experimental setup described by Dwivedi et al. (2023). We consider the ZINC dataset (Dwivedi et al., 2023) and use a 12K subset of the ZINC (250K) dataset (Irwin et al., 2012) with and without edge features. we employ

GIN (Xu et al., 2018), GCN (Kipf & Welling, 2017), PPGN (Maron et al., 2019a), DGN (Beaini et al., 2021), Deep LRP (Chen et al., 2020), and CIN (Bodnar et al., 2021) as baselines. The results are summarized in Table 10.

Methods	ZINC	
	Without Edge Features	With Edge Features
GCN	0.459 ± 0.006	0.321 ± 0.009
PPGN	0.407 ± 0.028	-
GIN	0.407 ± 0.028	0.163 ± 0.004
DGN	0.219 ± 0.010	0.168 ± 0.003
Deep LRP [#]	0.223 ± 0.008	-
CIN [#]	0.115 ± 0.003	0.079 ± 0.006
$\lambda_{\text{core-degree}}\text{-GPNN}^*$	0.214 ± 0.018	0.148 ± 0.015
$\lambda_{\text{core-degree}}\text{-GPNN}^\diamond$	0.222 ± 0.021	0.141 ± 0.011

Table 10: Graph regression MAE for ZINC 12K dataset. The best results are highlighted in **black** and the second best results are highlighted in **blue**. For the baseline results, we refer to (Bodnar et al., 2021). The methods marked by [#] are based on pre-selected domain-specific structural information.

From the results in Table 10, we can see that both GPNN variants show competitive performance in the regression task. Different from models like CIN, GPNN does not process any hand-crafted domain-specific structural information that is known to be highly correlated to molecular prediction tasks. Therefore, our model performance is less than such models.

C.5. Computational Resources

All our experiments are conducted on a Linux server with an Intel Xeon W-2175 2.50GHz processor alongside 28 cores, NVIDIA RTX A6000 GPU, and 512GB of main memory.

Dataset	Partitioning Scheme	# Partitions	Avg # Intra-Edges	Avg # Inter-Edges	# Intra-Edges / # Inter-Edges
ogbg-moltoxcast	Φ_{core}	3	5.08	33.44	13 / 87
	$\Phi_{\text{core-degree}}$	5	13.05	25.47	34 / 66
	$\Phi_{\text{core-onion}}$	42	24.53	13.99	64 / 36
	Φ_{degree}	7	24.56	13.96	64 / 36
	Φ_{triangle}	2	0.09	38.43	1 / 99
ogbg-moltox21	Φ_{core}	3	5.12	33.47	13 / 87
	$\Phi_{\text{core-degree}}$	5	13.18	25.41	34 / 66
	$\Phi_{\text{core-onion}}$	42	24.54	14.05	64 / 36
	Φ_{degree}	7	24.50	14.08	63 / 37
	Φ_{triangle}	2	0.09	38.50	1 / 99
ogbg-molhiv	Φ_{core}	4	7.09	47.84	13 / 87
	$\Phi_{\text{core-degree}}$	8	23.30	31.64	42 / 58
	$\Phi_{\text{core-onion}}$	88	33.53	21.41	61 / 39
	Φ_{degree}	11	33.52	21.42	61 / 39
	Φ_{triangle}	11	0.13	54.80	1 / 99

Table 9: Statistics for five graph partitioning schemes used in the experiments